Modeling and experimental studies of a side band power re-injection locked magnetron*

Wen-Jun Ye(叶文军), Yi Zhang(张益), Ping Yuan(袁萍),
Hua-Cheng Zhu(朱铧丞), Ka-Ma Huang(黄卡玛), and Yang Yang(杨阳)†

College of Electronics and Information Engineering, Sichuan University, Chengdu 610065, *China*

(Received 23 May 2016; revised manuscript received 17 August 2016; published online 25 October 2016)

A side band power re-injection locked (SBPRIL) magnetron is presented in this paper. A tuning stub is placed between the external injection locked (EIL) magnetron and the circulator. Side band power of the EIL magnetron is reflected back to the magnetron. The reflected side band power is reused and pulled back to the central frequency. A phase-locking model is developed from circuit theory to explain the process of reuse of side band power in SBPRIL magnetron. Theoretical analysis proves that the side band power is pulled back to the central frequency of the SBPRIL magnetron, then the amplitude of the RF voltage increases and the phase noise performance is improved. Particle-in-cell (PIC) simulation of a 10-vane continuous wave (CW) magnetron model is presented. Computer simulation predicts that the frequency spectrum's peak of the SBPRIL magnetron has an increase of 3.25 dB compared with the free running magnetron. The phase noise performance at the side band offset reduces 12.05 dB for the SBPRIL magnetron. Besides, the SBPRIL magnetron experiment is presented. Experimental results show that the spectrum peak rises by 14.29% for SBPRIL magnetron compared with the free running magnetron. The phase noise reduces more than 25 dB at 45-kHz offset compared with the free running magnetron.

Keywords: magnetrons, injection locking, tuning stub, phase noise

PACS: 84.40.Fe, 85.40.Qx, 84.30.Vn **DOI:** 10.1088/1674-1056/25/12/128402

1. Introduction

Magnetrons are widely used in many applications, such as radar, microwave heating and microwave chemistry. Magnetrons can supply a large range of power, from 1 kW to 100 kW at 915 MHz or 1 kW to 30 kW at 2.45 GHz.[1] Some projects, like the space solar power system (SSPS), need a very large number of high performance magnetrons, especially high-efficiency, low-noise, injection locked magnetrons.[2–4] However, as a crossed-field microwave device, the magnetron has intrinsic characteristics of wide band frequency spectrum and poor phase noise performance.[5–7] An effective method to improve the performance of the magnetron is the injection locking technique and the external injection locking (EIL) condition has been extensively studied.[8–11] Magnetron experiments with EIL method have also been investigated and show that its spectrum is improved compared with a free-running magnetron.[12–15] A self-injection locked magnetron can also reduce the phase noise compared with the free-running magnetron.[16,17]

In this paper, we propose a method to improve the output characteristics of the magnetron and we obtain better performance of frequency spectrum and phase noise than the EIL method. Theory and experiments about the side band power re-injection locked magnetron are presented. The theory analysis follows Slater's in Ref. [10], in which the magnetron-specific growth-saturation characteristic was discussed and Chen[11] who constructed the nonlinear frequency pushing effect in a relative magnetron. We adopt and expand their work in SBPRIL magnetron.

The rest of this paper is organized as following. In Section 2, theories about the RF voltage growth and phase noise reduction in SBPRIL magnetron are analyzed. The side band power's reflection and reabsorption are discussed. In Section 3, a 10-vane CW magnetron is simulated by Computer Simulation Technology Particle Studio (CST PS). In Sections 4 and 5, the first experimental demonstrations of both RF voltage increase and the phase noise reduction in the magnetron by using SBPRIL technique with Panasonic CW 2M244-M1 magnetron are presented. The 2M244-M1 magnetron is free running at 2.45 GHz and its output power can be adjusted from 200 W to 1 kW. A tuning stub is placed between the EIL magnetron and the circulator. The tuning stub acts as a bandpass filter. Side band power of the RF output of the EIL magnetron is reflected back to the magnetron. In Section 6, the numerical and experimental results are compared with each other.

2. Theoretical analysis

2.1. Amplitude and frequency behaviors of the free running and external injection locked magnetron

A magnetron is an oscillator essentially and the resonant cavity can be simplified into an RLC circuit. The RF voltage

*Project supported by the National Basic Research Program of China (Grant No. 2013CB328902) and the National Natural Science Foundation of China (Grant No. 61501311).

†Corresponding author. E-mail: yyang@scu.edu.cn

© 2016 Chinese Physical Society and IOP Publishing Ltd

(V_{RF0}) and frequency (ω') of the free running magnetron can be explained with Slater's mode:

$$V_{RF0} = \frac{V_{dc}}{1 + \dfrac{C\omega_0 R}{Q_L}}, \tag{1}$$

$$\omega' = \omega_0 + \frac{b_0}{2C} - \frac{B\omega_0}{2Q_{ext}} - \frac{\omega_0 \tan\alpha}{2Q_L}, \tag{2}$$

where V_{dc} is the dc-voltage between the cathode and the anode; C and R are the capacitor and the resistor in the equivalent circuit, respectively; ω_0 is the resonance frequency of the unloaded cavity; Q_{ext} and Q_L are the quality factors of the exterior and the load, respectively; b_0 is a constant; B represents the external load in the equivalent circuit; α is the frequency-pushing parameter which is typically of the order of unity; $b_0/2C - \omega_0 \tan\alpha/2Q_L$ represents the frequency pushing effect, which means that the frequency change is caused by the presence of the electron space charge; $B\omega_0/2Q_{ext}$ is the frequency pulling effect, which means that the frequency change is caused by the external load.

The RF voltage (V_{RF}) and frequency (ω) of the EIL magnetron can be explained with Chen's mode:

$$V_{RF} = V_{RF0}\frac{1}{1 + \dfrac{\rho\omega_0\cos\theta}{\gamma Q_{ext}}}, \tag{3}$$

$$\frac{d\theta}{dt} = \frac{\mu}{|\cos\theta|}\sin\theta + \sigma = 0, \tag{4}$$

where $\mu = \rho/Q_{ext}$, $\sigma = (\omega' - \omega_1)/\omega_0$,

$$\gamma = \frac{\omega_0}{2}\left(\frac{1}{Q_L} + \frac{1}{RC\omega_0}\right),$$

ρ is the injection ratio, ω_1 is the frequency of the external signal, $\theta = \omega t - \omega_1 t + \theta_0$, t is the time, and θ_0 is the relative phase difference between the output of the free running magnetron and the external signal.

By solving Eq. (4), one obtains

$$\tan\frac{\theta}{2} = \begin{cases} -\dfrac{\mu}{\sigma} + \dfrac{\sqrt{\mu^2-\sigma^2}}{\sigma}\dfrac{1-\exp(t\sqrt{\mu^2-\sigma^2})}{1+\exp(t\sqrt{\mu^2-\sigma^2})}, & \sigma > 0, \\ -\dfrac{\mu}{\sigma} - \dfrac{\sqrt{\mu^2-\sigma^2}}{\sigma}\dfrac{1-\exp(-t\sqrt{\mu^2-\sigma^2})}{1+\exp(-t\sqrt{\mu^2-\sigma^2})}, & \sigma < 0, \\ e^{2\mu t}, & \sigma = 0. \end{cases} \tag{5}$$

In Eq. (5), the Adler condition of injection locked magnetron[8] shows that $\mu \geq |\sigma|$, and t becomes infinite. So equation (5) becomes

$$\tan\frac{\theta}{2} = -\frac{\mu}{\sigma} - \frac{\sqrt{\mu^2-\sigma^2}}{\sigma}. \tag{6}$$

Then

$$\cos\theta = -\frac{1}{\mu}\sqrt{\mu^2-\sigma^2}. \tag{7}$$

So $\cos\theta$ in Eqs. (3) and (4) each always approach a negative value, then $V_{RF} \geq V_{RF0}$. This conclusion proves that the amplitude of the RF voltage can be increased in the EIL magnetron. To obtain the steady amplitude behavior of the EIL magnetron, we substitute the locking condition (4) into Eq. (3) by cancelling the dependence of θ , which leads to

$$\frac{\left(\dfrac{V_{RF0}}{V_{RF}} - 1\right)^2}{\left(\dfrac{\mu}{\gamma}\right)^2} + \left(\frac{\sigma}{\mu}\right)^2 = 1. \tag{8}$$

Equation (8) describes an ellipse curve and the $V_{RF}/V_{RF0} - \sigma$ curve is shown in Fig. 1 with $\gamma = 0.1$. The different curves represent the different values of the injecting parameter μ. The free running magnetron is represented with $\sigma = 0$ and $V_{RF}/V_{RF0} = 1$ as indicated by the dotted loop in Fig. 1. Considering that figure 1 is split into a stable part and an unstable part by a dashed-dotted line with the stable condition ($\cos\theta \leq 0$), figure 1 proves that the EIL magnetron frequency can be locked and the RF voltage can be increased.

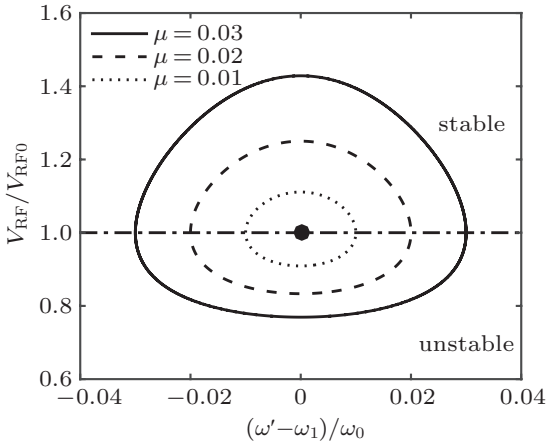


Fig. 1. Plots of amplitude (V_{RF}/V_{RF0}) versus frequency difference (σ) at three different injection parameters: $\mu = 0.01$, $\mu = 0.02$, and $\mu = 0.03$.

2.2. Side band power re-injection locked magnetron

The side band power re-injecting technique is based on the EIL method. From previous theory analysis, we prove that the frequency of the RF output can be coincident with the external signal frequency in EIL magnetron. The phase of the RF output can be controlled by the external injection signal. Specifically, the magnetron RF voltage always increases. Hence the RF spectrum can be improved. So, we suppose that if the sideband power is reflected back to the EIL magnetron, the RF voltage can increase more. In the SBPRIL magnetron, a tuning stub is placed between the EIL magnetron and the circulator to reflect the sideband power. Tuning stub, low Q value bandpass filter or high Q value bandpass filter can be obtained. The transfer function of the tuning stub is similar to

the bandpass filter[18]

$$H(\omega)=\frac{\mathrm{j}\omega\left(\frac{\omega_{\mathrm{r}}}{Q_{\mathrm{r}}}\right)}{(\omega_{\mathrm{r}}^2-\omega^2)+\mathrm{j}\omega\left(\frac{\omega_{\mathrm{r}}}{Q_{\mathrm{r}}}\right)}, \tag{9}$$

where ω_{r} is the central frequency of the bandpass filter and Q_{r} is the Q value of the bandpass filter. The real-word magnetron output signal which has phase noise can be written as

$$v(t)=A\sin(\omega_{\mathrm{l}}t+\phi(t)), \tag{10}$$

where $\phi(t)$ is the phase noise. We can simplify $\phi(t)$ into $A_0\sin(\omega_m t)$. Then

$$\begin{aligned} v(t) &= A\sin(\omega_{\mathrm{l}}t+A_0\sin(\omega_m t)) \\ &= AJ_0(A_0)\sin(\omega_{\mathrm{l}}t) \\ &\quad +AJ_1(A_0)[\sin(\omega_{\mathrm{l}}+\omega_m)t-\sin(\omega_{\mathrm{l}}-\omega_m)t] \\ &\quad +AJ_2(A_0)[\sin(\omega_{\mathrm{l}}+2\omega_m)t-\sin(\omega_{\mathrm{l}}-2\omega_m)t] \\ &\quad +\ldots, \end{aligned} \tag{11}$$

where $\mathrm{J}_n(Z)$ is the Bessel function of the first kind and its higher order terms each have a great attenuation. So we take the first two terms and define $\omega_{\mathrm{H}}=\omega_{\mathrm{l}}+\omega_m, \omega_{\mathrm{L}}=\omega_{\mathrm{l}}-\omega_m$. The unilateral Fourier transform of $v(t)$ is written as

$$\begin{aligned} V(\omega) &= \frac{A\pi}{\mathrm{j}}[\mathrm{J}_0(A_0)\delta(\omega-\omega_{\mathrm{l}}) \\ &\quad +\mathrm{J}_1(A_0)\delta(\omega-\omega_{\mathrm{H}})-\mathrm{J}_1(A_0)\delta(\omega-\omega_{\mathrm{L}})]. \end{aligned} \tag{12}$$

So the output of the tuning stub (when $\omega_{\mathrm{r}}=\omega_{\mathrm{l}}$) is

$$\begin{aligned} Y(\omega) &= H(\omega)V(\omega)=\frac{\pi}{\mathrm{j}}[\mathrm{J}_0(A_0)\delta(\omega-\omega_{\mathrm{l}}) \\ &\quad +H(\omega_{\mathrm{H}})\mathrm{J}_1(A_0)\delta(\omega-\omega_{\mathrm{H}}) \\ &\quad -H(\omega_{\mathrm{L}})\mathrm{J}_1(A_0)\delta(\omega-\omega_{\mathrm{L}})]. \end{aligned} \tag{13}$$

This means that the central frequency of the magnetron output (ω_{l}) passes through the tuning stub. Meanwhile, most of the side band power (ω_{L} and ω_{H}) is reflected back to the magnetron.

As shown in Fig. 2, firstly the magnetron is injecting-locked by a small power external signal. The frequency spectrum of the magnetron is shown in Fig. 2(a). Then, the tuning stub is placed between the magnetron and the circulator and the reflected signal's frequency spectrum is shown in Fig. 2(b). Because ω_{L} and ω_{H} are still in the locking bandwidth of the external signal ω_{l} , the reflected power is pulled back to the central frequency ω_{l} , then joins the RF output and increases the output power. We define the voltage ratio between SBPRIL magnetron (V_{RF}) and free running magnetron (V_{RF0}) as A. A_1, A_{L}, and A_{H} are the voltage ratios for $\omega_{\mathrm{l}}, \omega_{\mathrm{L}}$, and ω_{H} in Fig. 2(c), where $\sigma_{\mathrm{l}}=(\omega'-\omega_{\mathrm{l}})/\omega_0$, $\sigma_{\mathrm{L}}=(\omega_{\mathrm{L}}-\omega_{\mathrm{l}})/\omega_0$, $\sigma_{\mathrm{H}}=(\omega_{\mathrm{H}}-\omega_{\mathrm{l}})/\omega_0$. So, in the SBPRIL magnetron, the RF voltage is

$$V_{\mathrm{RF}}=A_1V_{\mathrm{RF1}}(\omega_{\mathrm{l}})+A_{\mathrm{L}}V_{\mathrm{RFL}}(\omega_{\mathrm{L}})+A_{\mathrm{H}}V_{\mathrm{RFH}}(\omega_{\mathrm{H}}). \tag{14}$$

Therefore, the RF voltage of the SBPRIL magnetron is increased by:

$$A=\frac{V_{\mathrm{RF}}}{V_{\mathrm{RF1}}}=A_1+A_{\mathrm{L}}\frac{V_{\mathrm{RFL}}(\omega_{\mathrm{L}})}{V_{\mathrm{RF1}}(\omega_{\mathrm{l}})}+A_{\mathrm{H}}\frac{V_{\mathrm{RFH}}(\omega_{\mathrm{H}})}{V_{\mathrm{RF1}}(\omega_{\mathrm{l}})}. \tag{15}$$

From Eq. (15), the increase of amplitude is related to

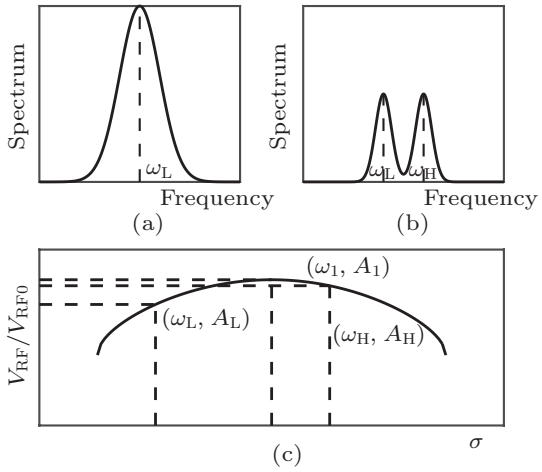


Fig. 2. Diagram of SBPRIL magnetron. (a) Spectrum of the EIL magnetron. (b) Spectrum of the reflected power. (c) The reflected power and the external signal getting different RF voltage amplitude.

(i) A_{L} and A_{H}, which depend on the frequency of the reflected power. If the tuning stub has a very high Q value, the frequency of the reflected signal is close to the central frequency and A_{L}, A_{H}, A_{L}, and A_{H} approach the maximum (A_1);

(ii) $V_{\mathrm{RF}}(\omega_{\mathrm{L}})$ and $V_{\mathrm{RF}}(\omega_{\mathrm{H}})$, which represent the reflected power. With a great reflected power, the more power is reclaimed.

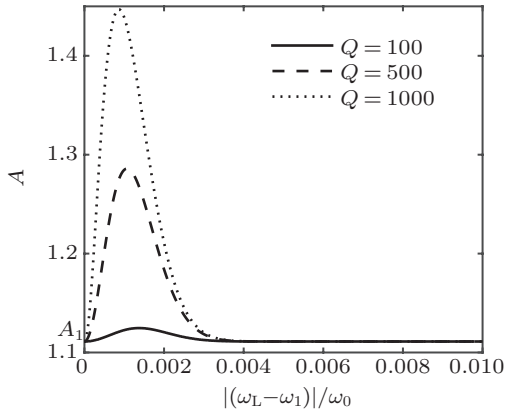


Fig. 3. Plots of amplitude ratio A versus the reflected power frequency difference with three different Q values of tuning stub.

The numerical analysis of A is shown in Fig. 3 with $\gamma=0.1$, $\mu=0.01$, and $\sigma_{\mathrm{l}}=0$. Meanwhile, we simplify the transfer function of the tuning stub into a symmetrical curve. So, $\sigma_{\mathrm{L}}=\sigma_{\mathrm{H}}$ and $A_{\mathrm{L}}=A_{\mathrm{H}}$. Figure 3 shows that when the tuning stub has a high Q value, the RF voltage ratio in the SBPRIL magnetron is greater.

3. Simulation verification

A 10-vane CW magnetron model is simulated in our work by using the Computer Simulation Technology Particle Studio (CST PS). The free running magnetron oscillates at 2.4496 GHz with the following parameters: anode voltage = −4200 V, anode current = 0.68 A, RF output voltage = 63.5 V, output power = 2 kW, and efficiency = 70.59%.

Figure 4 shows the external injecting signal and the frequency spectra of reflection side band power signal. The spectra of side band power shows that the central frequency of the RF output is filtered and the side band power is reflected back to the magnetron.

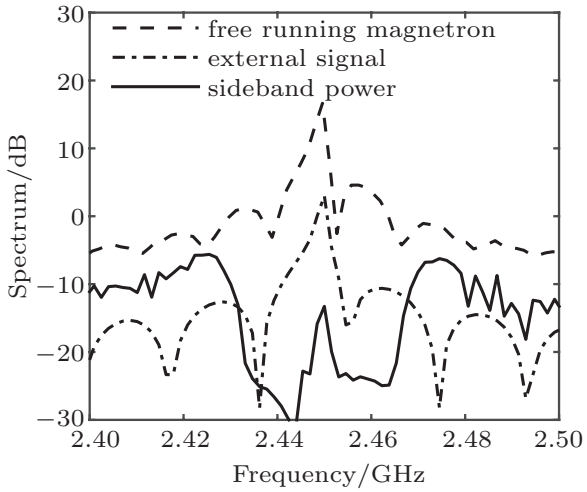


Fig. 4. Frequency spectra of the RF output of free running magnetron, the external signal, and the reflected side band power.

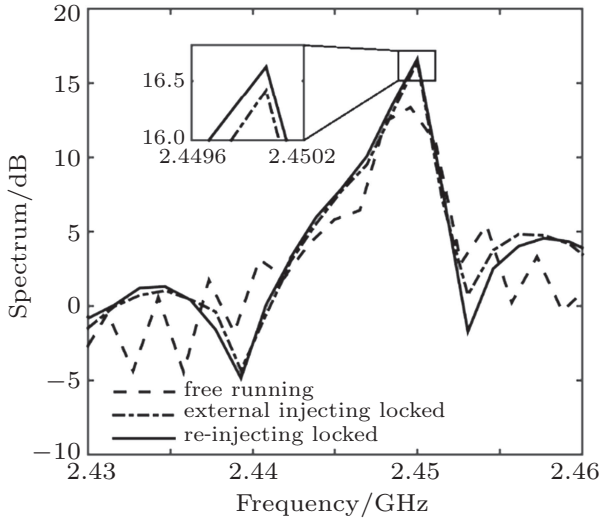


Fig. 5. Simulation frequency spectra of the three models of magnetron.

The three frequency spectra of the RF outputs of different models are shown in Fig. 5. The free running magnetron's frequency is pulled to the frequency of the external signal as shown in Fig. 5. The SBPRIL magnetron's frequency spectrum has a higher peak than the EIL magnetron's. The frequency spectrum's peak of free running magnetron is at 2.4496 GHz with 13.37 dB, the peak of EIL magnetron is at 2.45 GHz with 16.42 dB and the peak of SBPRIL magnetron is at 2.45 GHz with 16.62 dB. The frequency spectrum's peak of the SBPRIL magnetron has an increase of 3.25 dB compared with the free running magnetron's. Phase noise of the RF output is calculated and shown in Fig. 6. Phase noises of the EIL magnetron and the SBPRIL magnetron are reduced. Phase noise of the free running magnetron is −74.25 dBc/Hz, that of the EIL magnetron is −82.55 dBc/Hz, and that of the SBPRIL magnetron is −86.30 dBc/Hz at 3-MHz offset. The phase noise of SBPRIL magnetron is reduced by more than 12 dB at 3-MHz offset compared with the free running magnetron. Figures 5 and 6 illustrate that the side band power re-injected to the magnetron is pulled back to the central frequency of the SBPRIL magnetron and the RF output of the magnetron is increased and phase noise is improved.

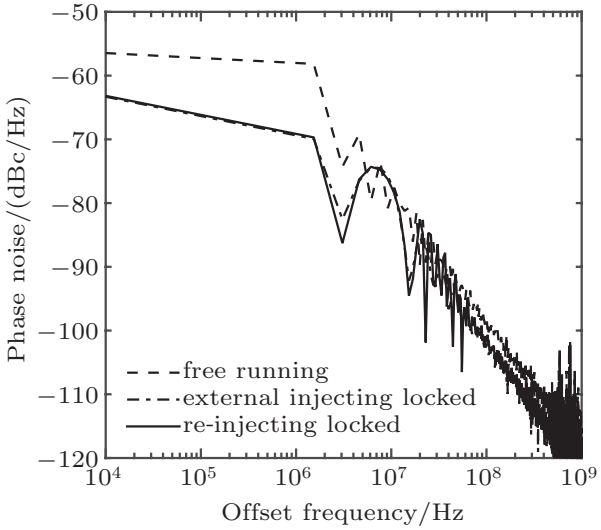


Fig. 6. Phase noises of the three models of magnetron.

4. Experimental setup

The experimental setup of the SBPRIL magnetron is shown in Fig. 7. In Fig. 7, an external signal source is used to supply an externally injected signal through the two circulators. The signal source is Hittite HMC-T2220 10 MHz–20 GHz signal generator. Reflected power is measured by power meter 1 and directional coupler 1. Output power is measured by the double directional coupler and the power meter 2. Frequency spectrum of the output is measured by the other coupler port of the double directional coupler. The power of external injecting signal is measured by directional coupler 2 and power meter 3. A practical setup of the SBPRIL magnetron experiment is shown in Fig. 8. The tested magnetron is Panasonic CW 2M244-M1. Frequency spectrum is measured by ROHED & SCHWARZ FSP spectrum analyzer and the power meter is AV2433.

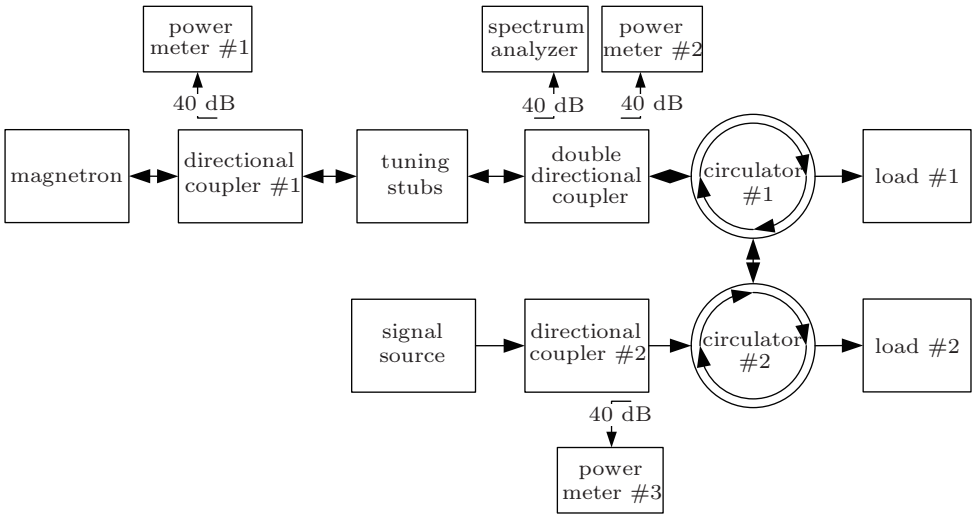


Fig. 7. The experimental schematic diagram.

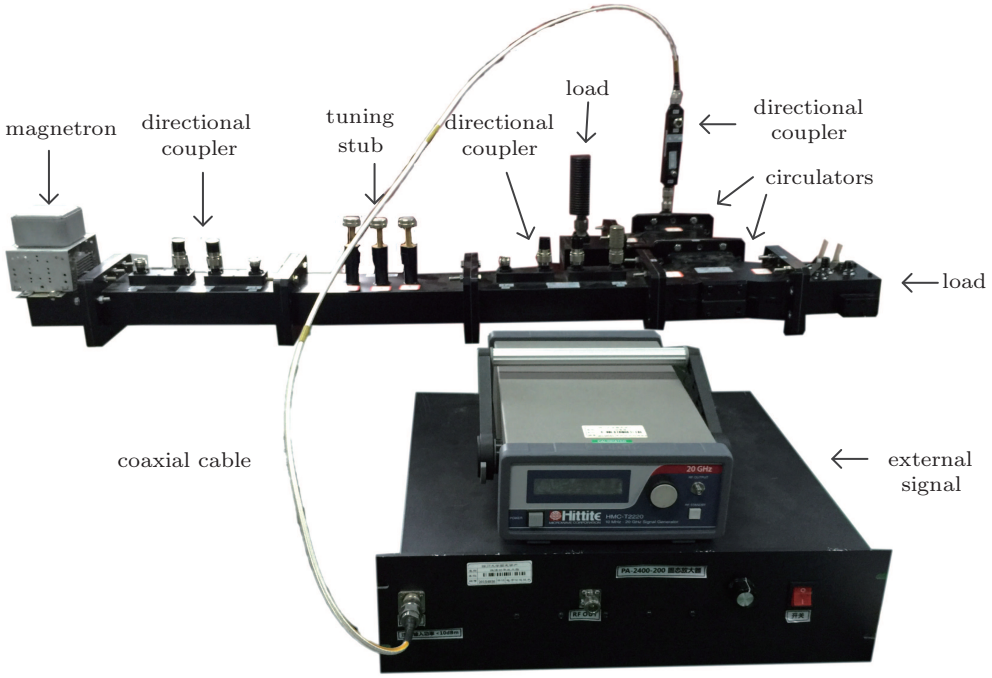


Fig. 8. (color online) Practical setup of the experiment.

5. Experimental results

5.1. Tuning stub in the free running magnetron

The tuning stub can optimize the power match of the magnetron to the circulator. So, the performance of free running magnetron with the tuning stub is tested first. In this test, the external signal source, directional coupler 2, circulator 2, and power meter 3 are removed. Load 2 is set up in the circulator 1. In the experiment, we adjust the three pins of the tuning stub at different positions. The depths of the three pins are adjusted from 0 mm to 5 mm, 10 mm, and 15 mm with respect to the waveguide wall. The spectrum peaks of the free running magnetron with the tuning stub at different positions are shown in Fig. 9. It shows that the spectrum peaks of the free running magnetron with tuning stub at different depths are lower than those of the magnetron with pins at their highest points. This means that the tuning stub can optimize the match between the magnetron and the circulator, but it cannot raise the RF output of the free running magnetron. Phase noises of the free running magnetron with tuning stub are measured and shown in Fig. 10. It shows that the effect of optimization on phase noise performance is weak. Phase noise can be a little lower, but it is increased in most cases. A comparison between the results in Fig. 9 and those in Fig. 10 shows that the tuning stub can indeed optimize the power match of the magnetron to the circulator to a small extent. But the tuning stub cannot improve the RF output nor phase noise performance in free running

magnetron.

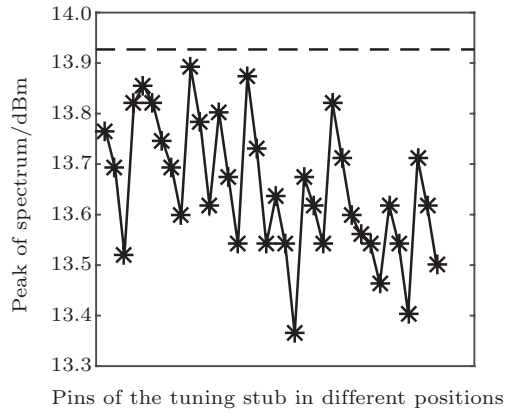


Fig. 9. Peaks of free running magnetron with tuning stub. The dashed line is the peak of free running magnetron with all the three pins at their highest points and the tuning stub is used as a directional waveguide. The solid data point-fold line is the peak of free running magnetron with pins at different positions. In those operating conditions, the tuning stub is an optimizer.

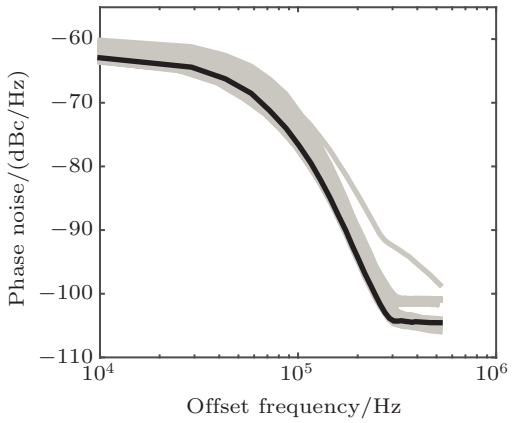


Fig. 10. Phase noise of free running magnetron with tuning stub. The black line is all three pins at their highest points and the tuning stub is used as a directional waveguide. Gray lines are the three pins at different depths and the tuning stub is an optimizer.

5.2. Tuning stub in the SBPRIL magnetron

In Figs. 9 and 10, the optimizer effect of the tuning stub cannot raise the RF voltage and cannot improve the phase noise performance of the free running magnetron either. So, in the experiment of the SBPRIL magnetron, the tuning stub is adjusted to be used as a bandpass filter. Figure 11 shows the scatter parameters of the tuning stub in experiment. The tuning stub acts as a band pass filter. But its Q value is very low.

In the experiment, the free running magnetron oscillates at 2.4499 GHz with the following operating parameters: anode voltage = −4048 V, anode current = 146.2 mA, heater voltage = 3 V, heater current = 8 A, output power = 353 W, and peak of spectrum= 14.21 dBm. The external signal frequency is set to be 2.45 GHz and its power is 20 W. So the EIL magnetron oscillates at 2.45 GHz with following operation parameters: cathode voltage = −4031 V, anode current = 146.2 mA, heater voltage = 3 V, heater current = 8 A, output power = 372W, peak of spectrum = 14.52 dBm. Then, the tuning stub is adjusted to the operating conditions as shown in Fig. 11. The tuning stub reflects the side band power and the reflected power is 40 W. The SBPRIL magnetron oscillates at 2.45 GHz with the following operating parameters: cathode voltage = −4008 V, anode current = 146.2 mA, heater voltage = 3 V, heater current = 8 A, output power = 375 W, and peak of spectrum = 14.79 dBm.

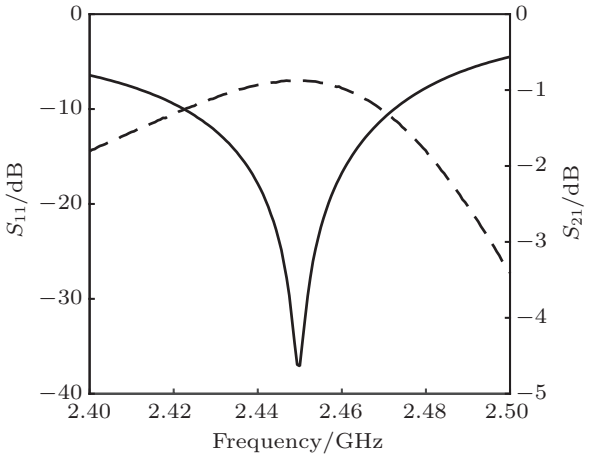


Fig. 11. The Scatter parameters of the 3-stub tuner. Solid curve is for S_{11} and dashed curve is for S_{21}.

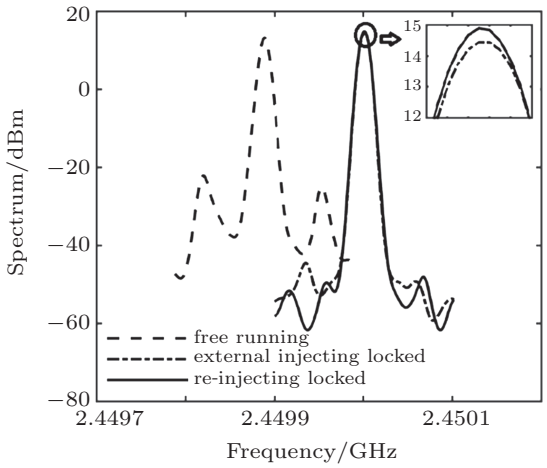


Fig. 12. Experimental frequency spectra of the magnetron under three different operating conditions.

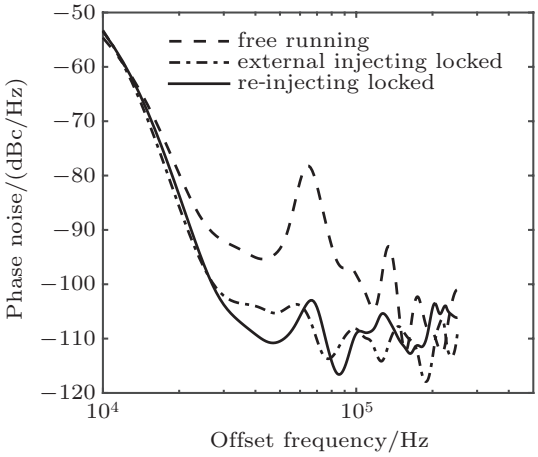


Fig. 13. Experimental phase noises of the magnetron under three different operating conditions.

Figures 12 and 13 show the experimental frequency spectra and phase noise performances of the magnetron under three operating conditions. The resolution bandwidth of the spectrum analyzer is set to be 30 kHz and the video bandwidth is set to be 10 kHz. The frequency spectra in Fig. 12 show that the reflected side band power is pulled to the external injection signal frequency afresh. The side band spectrum is lower and the peak goes up from 14.21 dBm to 14.79 dBm with a 14.29% increase. Figure 13 shows that the phase noise performance has also confirmed the previous conclusion. The EIL magnetron and the SBPRIL magnetron both reduce the phase noise and the phase noise performance for SBPRIL magnetron is better than that for the EIL magnetron. In particular, the phase noises for the free running magnetron are −65.1 dBc/Hz at 45-kHz offset and −74.8 dBc/Hz for EIL magnetron, respectively. Phase noise of SBPRIL magnetron further reduces 5.6 dB to −80.4 dBc/Hz at 45-kHz offset. The efficiencies of the magnetrons in three states are tested and listed in Table 1. The efficiencies of EIL magnetron and SBPRIL magnetron both increase and the efficiency of the SBPRIL magnetron increases more than that of the EIL magnetron.

Table 1. Detailed parameters of the magnetrons under three different operating conditions.

Operating condition	Reflected power/W	External inject power/W	Output spectrum peak/dBm	Phase noise at 45-kHz offset/(dBc/Hz)	Efficiency
Free running magnetron	–	–	14.21	–65.1	59.6%
EIL magnetron	–	20	14.52	–74.8	63.1%
SBPRIL magnetron	40	20	14.79	–80.4	64.0%

6. Conclusions

In this paper, SBPRIL magnetron is presented. The side band power is reflected back to the magnetron. The circuit model is presented to analyze the RF voltage growth and frequency pulling effect in the SBPRIL magnetron. Theory analysis indicates that the side band power is reused and the RF voltage of SBPRIL magnetron increases more than that of the EIL magnetron (Figs. 2 and 3). The RF voltage increase is affected by the injection ratio ρ, the frequency difference between the external signal and the free running magnetron σ, and the Q value of the tuning stub.

PIC simulation for a 2.45-GHz, 2-kW CW magnetron is presented. Simulation results show that the frequency spectrum peak of SBPRIL magnetron increases 3.25 dB compared with that of the free running magnetron (in Fig. 5). The phase noise of the SBPRIL magnetron is reduced by more than 12 dB at 3 MHz offset compared with that of the free running magnetron.

Experiments with 2.45-GHz microwave oven magnetron are conducted. The optimizer effect of the tuning stub is excluded at first. The experimental results of the SBPRIL magnetron show that the RF frequency spectrum is raised up by 14.29% (in Fig. 12), the phase noise is reduced by 25.3 dB at 45 kHz offset (in Fig. 13). The frequency spectrum of SBPRIL magnetron has higher peak and better phase noise performance than that of free running magnetron. This conclusion confirms the theoretical analysis in Section 2. The SBPRIL magnetron has more concentrated spectrum and better phase noise performance at low cost. So it is very suitable for industrial applications of high-power microwave.

Acknowledgment

The authors would like to thank Sichuan Injet Electric Co. Ltd for the DC power supply of magnetron.

References

[1] Vyas S K, Maurya S and Singh V P 2014 *IEEE Trans. Plasma Sci.* **42** 3373
[2] Tahir I, Dexter A and Carter R 2005 *IEEE Trans. Electron Dev.* **52** 2096
[3] Dexter A C, Burt G and Carter R G 2011 *Phys. Rev. Accel. Beams* **14** 032001
[4] SShinohara N, Matsumoto H and Hashimoto K 2003 *Asia Pacific Microwave Conference*, 2003, Tokyo, Japan, p. 1550
[5] Collins G B 1948 Microwave Magnetron (New York: McGraw-Hill) pp. 698–738
[6] Yamamoto K, Kurobuma H, Koinuma T and Tashiro N 1987 *IEEE Trans. Electron Dev.* **34** 1223
[7] Osepchuk J M 1995 *Proc. 1st Int. Workshop on Crossed-Field Devices*, 1995, Ann Arbor, USA, p. 159
[8] Adler R 1946 *Proc. IEEE* **61** 351
[9] Slater J C 1946 *Rev. Mod. Phys.* **18** 441
[10] Slater J C 1947 *Tech. Rep.* **35** 1
[11] Chen S C 1990 *IEEE Trans. Plasma Sci.* **18** 570
[12] Pengvanich P, Neculaes V B, Lau Y Y, Gilgenbach R M, Jones M C, White W M and Kowalczyk R D 2005 *J. Appl. Phys.* **98** 114903
[13] Tahir I, Dexter A and Carter R 2006 *IEEE Trans. Electron Dev.* **53** 1721
[14] Treado T A, Hansen T A and Jenkins D J 1991 *14th Biennial Particle Accelerator Conference: Accelerator Science and Technology*, 1991, San Francisco, USA, p. 702
[15] Yue S, Zhang Z C and Gao D P 2014 *Chin. Phys. B* **23** 088402
[16] Choi J J and Choi G W 2007 *IEEE Trans. Electron Dev.* **54** 3430
[17] Sze H, Smith R R, Benford J N and Harteneck B D 1992 *IEEE Trans. Electromagn. Compat.* **34** 235
[18] Chang H 2003 5 *IEEE Trans. Microwave Theory Tech.* **1** 1994